remote sensing

MDPI

Technical Note

Simulation of Transient Topside Layer in the Martian Ionosphere

Chunhua Jiang *, Rong Tian and Lehui Wei

Department of Space Physics, School of Electronic Information, Wuhan University, Wuhan 430072, China
* Correspondence: chuajiang@whu.edu.cn; Tel.: +86-13986190965

Abstract: Many Mars missions, e.g., Mariner, Viking, Mars Global Surveyor (MGS), Mars Express (MEX), and Mars Atmosphere and Volatile Evolution (MAVEN), have been launched to study the Martian atmosphere. These observations have improved our understanding of the ionosphere of Mars. Observations show that the Martian ionosphere could be divided into an M2 layer (at ~140 km altitude) and an M1 layer (at ~110 km altitude), ionized by EUV and X-ray solar radiation, respectively. However, there are still many scientific questions about the Martian ionosphere. A transient topsider layer (also called the M3 layer, at ~160–~220 km) can frequently be measured above the M2 layer in the Martian ionosphere. The statistical characteristics of the M3 layer show that it is not irradiated by solar incident radiation. Many candidate mechanisms have been suggested to explain the formation of the M3 layer. However, the method of describing or modeling the M3 layer is still one of the many open scientific questions about the Martian ionosphere. This study used a one-dimensional model, including photochemical production, loss, and dynamic transport processes to simulate the transient topside layer in the Martian ionosphere. The M3 layer was reproduced by a perturbed vertical plasma drift in this study. The enhancement of the electron temperature induced by the dynamic process of plasma could facilitate the formation of the M3 layer. Our results show that the vertical transport process of plasma might be more crucial in producing the M3 layer in the topside Martian ionosphere.

Keywords: transient topside layer; Martian ionosphere; M3 layer; simulation

Citation: Jiang, C.; Tian, R.; Wei, L. Simulation of Transient Topside Layer in the Martian Ionosphere. *Remote Sens.* **2023**, *15*, 770. https://doi.org/10.3390/rs15030770

Academic Editors: Lin Li, Yuanzhi Zhang and Shengbo Chen

Received: 21 December 2022
Revised: 22 January 2023
Accepted: 25 January 2023
Published: 29 January 2023

1. Introduction

In the past several decades, many missions to Mars, e.g., Mars Express [1], MGS [2], and MAVEN [3], have improved our understanding of the atmosphere of Mars. The Martian ionosphere, as an important part of the upper atmosphere, has also been further investigated. The altitudinal structure of the Martian ionosphere is similar to that of the terrestrial ionosphere. The regular electron density profile of the Martian ionosphere can be divided into the M2 and M1 layers [4]. The M2 layer is mainly generated by EUV photoionization, and it is located ~140 km above Mars. The maximum electron density can be found in the M2 layer. The M2 layer varies with the solar zenith angle (SZA). The M1 layer is located below the M2 layer (~30 km lower than M2 layer). Higher-energy X-ray photons play a significant role in the formation of the M1 layer. Similarly, the M1 layer varies with the SZA. The metal ion layer, similar to the sporadic E-layer (Es layer) on Earth, can be observed due the meteoric ablation [5,6]. It mainly occurs below the M1 layer. In the topside ionosphere of Mars (above the M2 layer), a topside layer (or "bulge"), created by local enhancements of the electron density, can occasionally be measured at ~160–~220 km [7–9].

A simulation of the photochemical production and loss process can reproduce the M1 and M2 layers in the Martian ionosphere. However, the manner by which to produce the M3 layer in the Martian ionosphere is still unknown. Many candidate mechanisms have been suggested an explanations for the formation of the M3 layer., including solar wind [10,11], plasma instabilities [12–14], a crustal magnetic field [15,16], plasma temperature [17], Joule

heating [18], wave-like structures [19–21], etc. Mayyasi et al. [8] analyzed MGS Radio occultation data (about 5600 ionospheric profiles) to investigate the characteristics of the M3 layer. They found that the M3 layer did not vary with the solar zenith angle, solar irradiances, or seasons. These characteristics of the M3 layer are inconsistent with some popular explanations that rely on plasma instabilities, a crustal magnetic field, etc. They might suggest that the main driver of the M3 layer has still not been revealed and requires further study. Mendillo et al. [22] further suggested that the altitudinal variations in the electron temperature (enhancements in the 160–175 km region) might play an important role in the formation of the M3 layer. Following the work of Mayyasi et al. [8], Mukundan, et al. [9], studied the properties of the M3 layer (dayside ionospheric profiles) as measured by the Radio Occultation Science Experiment (ROSE) on MAVEN. They focused on two widely-cited possible mechanisms (electron temperature and a crustal magnetic field). The results found by Mukundan et al. [9] suggested that both electron temperature and crustal magnetic field might not play significant roles in the formation of the M3 layer.

A comparative study of the terrestrial and planetary ionospheres might improve our understanding of the planetary ionosphere. On Earth, the F3 layer above the regular F2 layer can occasionally be observed in the ionosphere in the equatorial and low-latitude regions. The large vertical ExB drift plays a critical role in the formation of the F3 layer in the terrestrial ionosphere [23]. In addition, gravity waves from the lower atmosphere can also affect the structure of the ionosphere [24,25]. Different from the F3 layer mentioned above, the F2 layer could be stratified and also form a new layer. In any case, both of the driver forces can affect the vertical dynamic process of plasma in the ionosphere. Then, a new additional layer can be produced. The physical mechanism of the F3 layer or F2-layer stratification (the vertical dynamic process) might give us a candidate for an inspired reason for the M3 layer in the Martian ionosphere. In the present study, a one-dimensional model, which includes photoionization production and loss and dynamic processes, was developed to simulate the M3 layer in the Martian topside ionosphere. It could help us further understand the physical process involved in the formation of the M3 layer.

2. Model of Daytime Martian Ionosphere and Descriptions

In this study, a one-dimensional model was developed to solve O_2^+, CO_2^+, O^+, and N_2^+ continuity equations for the photoionization production and loss and the dynamic transport processes:

$$\frac{\partial N}{\partial t} + \nabla \cdot (N\vec{V}) = P - L \quad (1)$$

where N represents the density of ions, $\vec{V}$ represents the vertical velocity of ions, P represents production rates, and L represents ion-loss processes.

The ions in the Martian lower ionosphere are mainly produced through photoionization and chemical reactions. Solar radiation is the source of the photoionization, and the neutral components of the atmosphere absorb the solar extreme ultraviolet (EUV) radiation and part of the X-rays to produce the ions. Table 1 (a–b) shows the reaction equations associated with solar radiation in the Martian atmosphere. At the same time, various chemical reactions can occur between ions and ions, as well as between ions and electrons, resulting in changes in their density. Table 1 (d–n) shows the chemical reactions and their reaction rates as used in this model.

Table 1. The reaction equations and their reaction rates used in the present model [26].

Reaction	Rate Constant, cm^3/s
(a) $CO_2 + h\nu \rightarrow CO_2^+ + e^-$	
(b) $O + h\nu \rightarrow O^+ + e^-$	
(c) $N_2 + h\nu \rightarrow N_2^+ + e^-$	
(d) $CO_2^+ + O \rightarrow O^+ + CO_2$	$k1 = 9.6 \times 10^{-11}$
(e) $CO_2^+ + O \rightarrow O_2^+ + CO$	$k2 = 1.6 \times 10^{-10}$
(f) $N_2^+ + CO_2 \rightarrow CO_2^+ + N_2$	$k3 = 8.0 \times 10^{-10}$
(g) $N_2^+ + O \rightarrow O^+ + N_2$	$k4 = 9.8 \times 10^{-12}$
(h) $N_2^+ + O \rightarrow NO^+ + N$	$k5 = 1.3 \times 10^{-10}$
(i) $O^+ + N_2 \rightarrow NO^+ + N$	$k6 = 1.2 \times 10^{-12}$
(j) $O^+ + CO_2 \rightarrow O_2^+ + CO$	$k7 = 1.1 \times 10^{-9}$
(k) $CO_2^+ + e^- \rightarrow CO + O$	$\alpha_1 = 3.1 \times 10^{-7} \times \left(\frac{300K}{T_e}\right)^{0.5}$
(l) $N_2^+ + e^- \rightarrow N + N$	$\alpha_2 = 2.2 \times 10^{-7} \times \left(\frac{300K}{T_e}\right)^{0.39}$
(m) $O_2^+ + e^- \rightarrow O + O$	$\alpha_3 = 1.95 \times 10^{-7} \times \left(\frac{300K}{T_e}\right)^{0.7}$, $T_e < 1200K$
(n) $NO^+ + e^- \rightarrow N + O$	$\alpha_4 = 4.0 \times 10^{-7} \times \left(\frac{300K}{T_e}\right)^{0.5}$

Mayyasi et al. [8] found that the plasma of the M3 layer does not respond to variations in SZA, solar irradiances, or seasons. Therefore, the averaged values of solar irradiance and neutral components measured by MAVEN in 2018 were used as the input for this model. In this study, we averaged the measured irradiance of MAVEN in 2018 to create a new irradiance model by using the same wavelength bin as SOLAR2000 [27]. This enables the avoidance of the SOLAR2000 model's potential inaccuracies associated with calibrating the effect of solar rotation and orbital variations. Furthermore, the model obtained the absorption and ionization cross-sections for bins #3–39 from Schunk and Nagy [26]. The other two bin values were obtained from Verner and Yakovlev [28] and Verner et al. [29], respectively [22]. Figure 1 shows the solar irradiance values from different wavelength bins used in this model. In this study, we used three main neutral components, CO_2, N_2, and O, which were obtained by averaging the data measured by the neutral component of the MAVEN NGIMS in 2018. The approximate solution of Equation (1) is achieved by using finite difference methods. Centered differences were used on the interior points, and forward differences were used for the border points. The heights range from 125 to 300 km. At first, the grid-spacing altitude was set to 1 km, 0.5 km, and 0.1 km, respectively, to test the numerical convergence study of the finite difference methods. We considered the cost of the running time and the fact that the velocity of plasma is less than 20 m/s in this study. The grid-spacing altitude was set to 1 km, and the running time step was set to 0.01 s in this model, which might be accurate enough for this study. Four ion densities of O_2^+, CO_2^+, O^+, and N_2^+ were obtained. The electron density profile was then calculated by adding all four ion densities together. The electron temperature used in this model was the average electron temperature as measured by MAVEN during 2018. At first, only the processes of photoionization production and loss were considered as we carried out simulation of the background of the Martian ionosphere. Then, the transport process can be added to the simulation of transient topside layer.

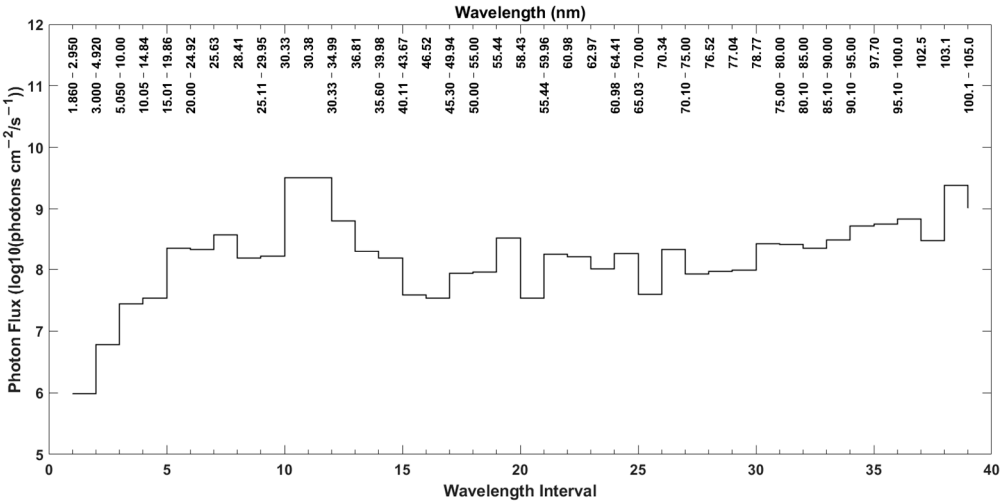

Figure 1. Solar irradiance values (log10(photons cm^{-2}/s^{-1})) from different wavelength bins used in this model.

Morgan et al. [30] used the ionospheric traces collected by MARSIS over the course of 2 years (from 14 August 2005 to 31 July 2007) to fit the Chapman ionospheric model. Three parameters (maximum electron density, electron density altitude, and neutral scale height) were estimated from the MARSIS data. Then, electron profiles were estimated from the Chapman ionospheric model (an analytical photochemical theory); the electron density N is given by:

$$n_e = n_0 \exp\left\{0.5 \cdot \left[1 - \frac{h - h_0}{H} - Ch(\chi) \exp\left(-\frac{h - h_0}{H}\right)\right]\right\} \quad (2)$$

where h is the altitude, H is the neutral scale height of the planetary atmosphere, χ is the solar zenith angle, n_0 is the subsolar maximum electron density, h_0 is the altitude of the subsolar maximum electron density, and Ch is the Chapman grazing incidence function. Morgan et al. [30] used ionospheric traces collected between August 2005 and July 2007 to fit to the Chapman ionospheric model. Their results showed that the value of n_0 varies from $n_0 = 1.4 \times 10^5$ cm^{-3} to $n_0 = 1.8 \times 10^5$ cm^{-3}, h_0 varies from 115 km to 135 km, and H varies from 11 km to 17 km [30].

Although the years of the MARSIS data (August 2005–July 2007) used in the Chapman model and the MAVEN data (2018) used in the present model are different, the solar irradiances in these two periods are comparable. Therefore, the electron profiles estimated from the present model were compared with those from the Chapman model [30] at different SZAs to test the performance of our model. In this study, the parameters of the Chapman model were set as $n_0 = 1.76 \times 10^5$ cm^{-3}, $h_0 = 125$ km, and $H = 11$ km for the Martian ionosphere.

Figure 2 shows the variations of the electron density profile with the solar zenith angle according to this model, and Equation (2) fits the MARSIS data. The results show that the electron density profiles matched well with the Chapman layer near the peak altitude and bottomside ionosphere, especial for the low SZA cases. In the topside ionosphere, the discrepancy was larger than in the bottomside ionosphere. Vogt et al. [31] also used ionospheric data from MAVEN to fit the Chapman layer. Their results (see Figure 5 in Vogt et al. [31]) showed that the Chapman layer mostly underestimated the topside electron density. It is well-known that the Chapman layer mainly represents photochemical equilibrium in the ionosphere. To further validate the performance of the present model, observations taken by ROSE on MAVEN in 2018 were also compared with the simulations. Figure 3 shows the comparison between observations from ROSE on MAVEN and the simulations. We found that there are some differences between them, especial for SZA = 60°. It should be noted that the number of electron profiles from ROSE (about 180 profiles, and less than 20 profiles for SZA = 60°) are rare for 2018. However, there are about 12,291 yield-

acceptable profile fits to the Chapman ionospheric model [30]. Therefore, it might be reasonable that the Chapman ionospheric model proposed by Morgan et al. [30] was used to estimate the performance of this model. As a result, the electron density estimated by the present model might be reasonable in our study.

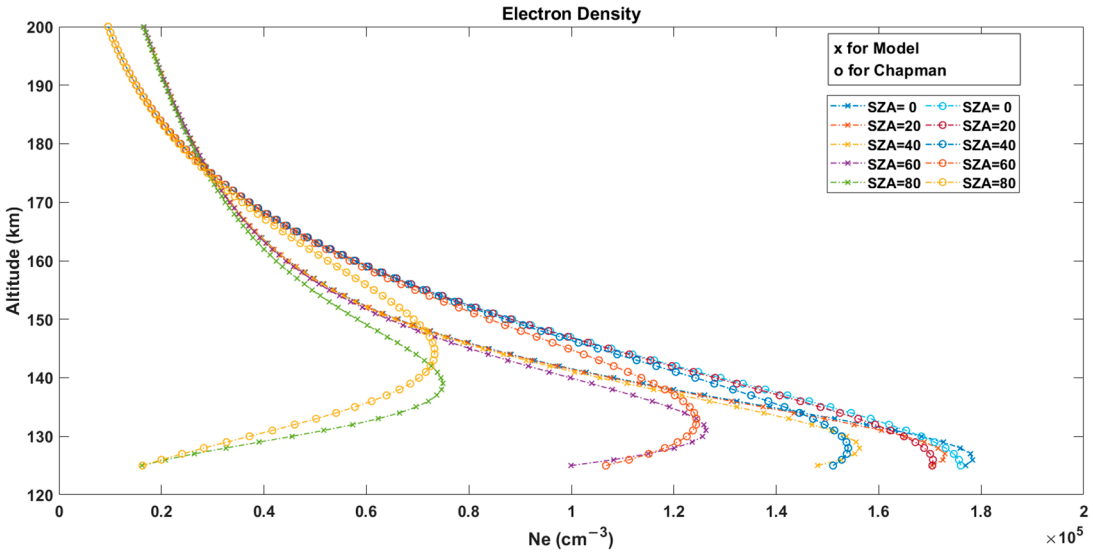

Figure 2. Variations of electron density profiles with SZA estimated from the model (marker with 'x') and the Chapman layer (marker with 'o').

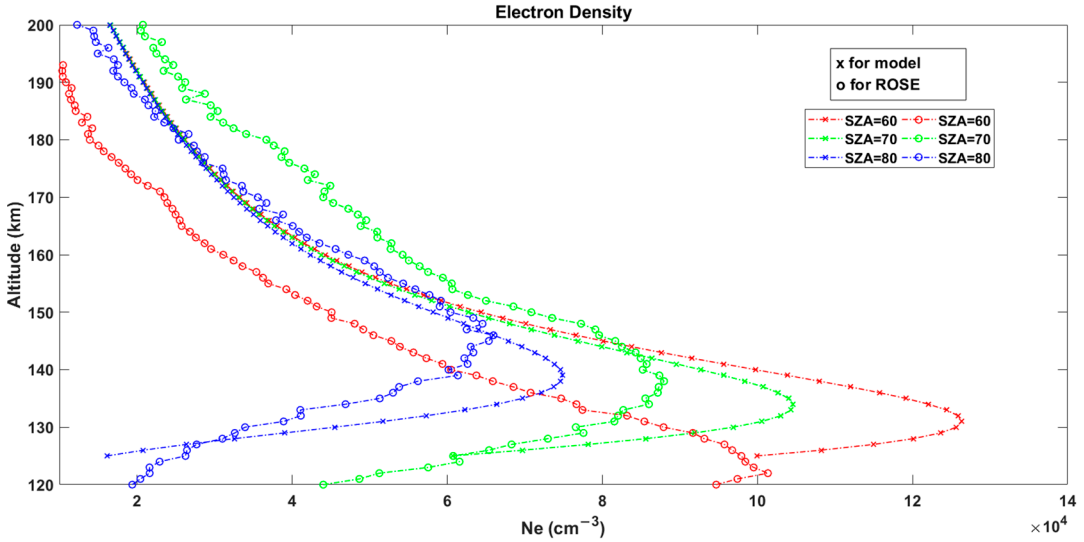

Figure 3. Variations of electron density profiles, with SZAs estimated by the model (marked with "x") and from ROSE on MAVEN (marked with "o").

3. Results and Discussion

Both Mayyasi et al. [8] and Mukundan et al. [9] carried out statistical studies of the characteristics of the M3 layer using the Mars Global Surveyor (MGS) radio occultation data set and the MAVEN ROSE observations, respectively. Mayyasi et al. [8] proposed that the M3 layer's plasma does not respond to variations in the solar zenith angle, solar irradiances, or seasons. Mukundan et al. [9] also found that the M3 peak density is insensitive to the SZA. Both M3 peak density and altitude were found to show no latitudinal dependence [9]. Therefore, in this simulation, the SZA was set to 60 degrees to represent a typical case. In the vertical transport process in the Martian ionosphere, only the perturbation vertical velocity of plasma was considered for the simulation of the transient topside layer.

Figure 4 shows the initial electron temperature (Figure 4a); densities of the O_2^+, CO_2^+, O^+, and N_2^+ electrons (Figure 4b); and the perturbed vertical velocity of the plasma (Figure 4c) profiles in the running model. The initial electron temperature is the average electron temperature measured by MAVEN during 2018. The initial electron density is derived from the equilibrium state of the photoionization production and loss processes with SZA = 60 and the initial electron temperature. The maximum disturbed vertical velocity is set to 20 m/s at 165 km in the topside Martian ionosphere. Yiğit et al. [32] reported that the Martian thermospheric GW activity varies strongly with the altitude and could reach a maximum perturbation at ~170 km. Therefore, it might be reasonable that the maximum disturbed velocity is set at 165 km in this simulation.

In this simulation, two cases were run to determine the role of the electron temperature in the formation of the M3 layer. Table 2 shows the two cases with different conditions. The electron temperature was set to be constant in the first case. In the second case, we assumed that electron temperature was in the equilibrium state before considering the disturbed vertical transport of the plasma. Other than the simulations of the electron temperature by Matta et al. [33], only the effect of the disturbed vertical transport process of ions (or electrons) on the electron temperature was be considered.

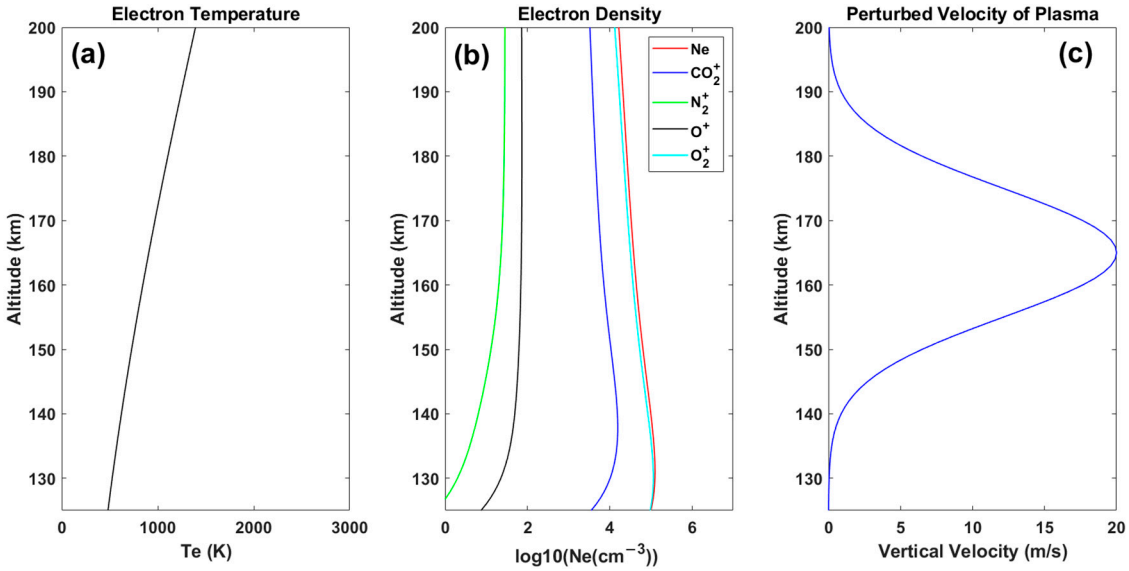

Figure 4. Initial parameters for the model in this study. (**a**) electron temperature; (**b**) densities of O_2^+, CO_2^+, O^+, and N_2^+ electrons; (**c**) disturbed vertical upward velocity of plasma.

Table 2. Run modes of the simulation with different parameters.

Run Modes	Description
Case 1	Electron temperature is constant in the simulation.
Case 2	Electron temperature varies with the gradients of the electron temperature and vertical velocity, $\frac{\partial T_e}{\partial t} = -\frac{2}{3}T\frac{\partial V}{\partial z} - V\frac{\partial T_e}{\partial z}$.

Figure 5 shows the altitudinal variations in electron density and temperature in the present simulation. We found that the transient topside layer could be reproduced in the topside Martian ionosphere. Case 1, as shown in Figure 5, demonstrates that the transient topside layer (the M3 layer, located at about 170~180 km) could be simulated although there were no enhancements of the electron temperature. It suggested that the vertical transport induced by the perturbed vertical velocity of the plasma could also produce the M3 layer. In Case 2, with the development of plasma transport in the Martian ionosphere,

the electron temperature increased in the region of ~175–200 km and decreased in the region of ~135–175 km (Figure 5). Figure 5 shows the transient topsider layer (the M3 layer, located at about 180 km) more obviously in Case 2 than in Case 1. Apparently, the enhancement of the electron temperature facilitates the formation of the M3 layer. In the present simulation, the maximum altitude is, respectively, about 175 km and 180 km in Cases 1 and 2, respectively. The peak concentration of the M3 layer is about 4×10^4 cm^{-3}. Figure 6 shows the densities of the O_2^+, CO_2^+, O^+, and N_2^+ electrons in Case 1 (left) and Case 2 (right) at a running time of t = 1000 s. It can be seen from Figure 6 that the M3 layer could also be observed in the main ion (O_2^+), but it is not obvious in the other ions. Figure 7 shows the variation of electron density with the running time used in this model. The results show that the M3 layer started to occur at about t = 400 s and at t = 300 s in Cases 1 and 2, respectively. Figure 7 further suggests that the M3 layer is more obvious in Case 2 than in Case 1. Mayyasi et al. [8] reported that the M3 layer has an average peak concentration of $9 \times 10^3 \pm 3.8 \times 10^3$ cm^{-3}, which is mainly located at 175 ± 11 km. The altitude of the M3 layer in this simulation is consistent with those observations. The peak concentration of the M3 layer is larger than in those observations. In the region of the M3 layer (about 175 km), the electron concentration is about 3×10^4 cm^{-3} in the background topside ionosphere (See Figure 4b). That is the reason that there are some slight differences in peak concentrations between the simulations and the observations. This might suggest that the photoionization process of the model overestimates the electron density in the topside ionosphere. However, the dynamic process of the model was able to reproduce the M3 layer above the M2 layer. It is still valuable to help understand how the M3 layer is produced above the M2 layer in the Martian ionosphere.

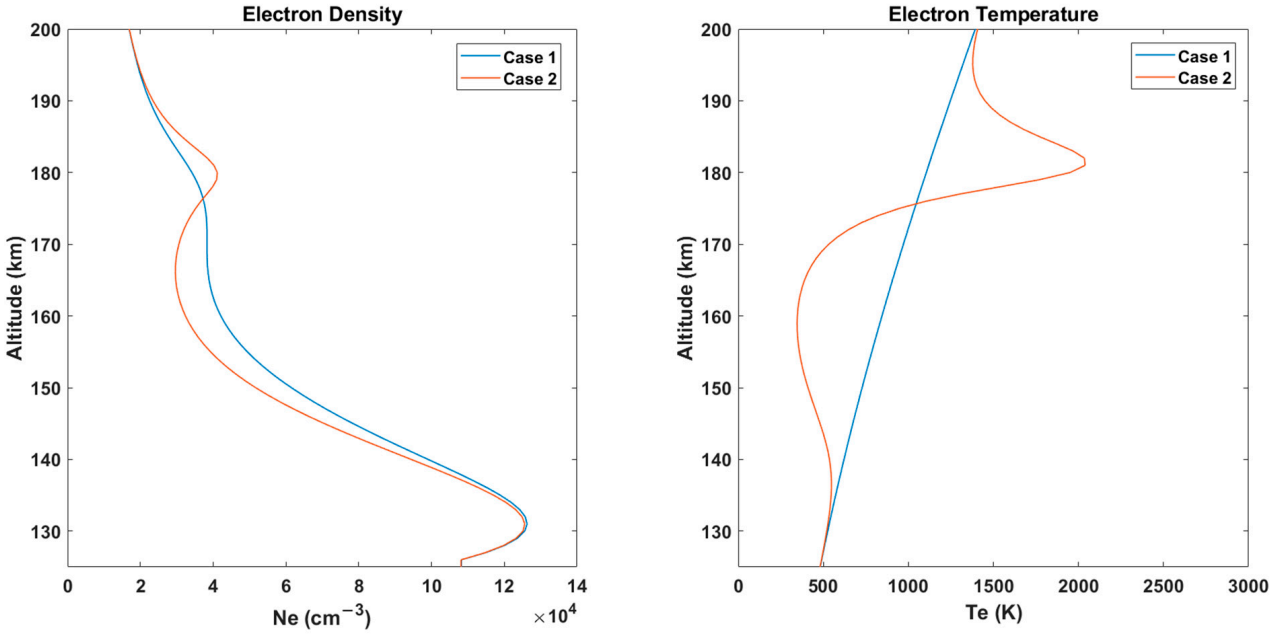

Figure 5. Variations in electron density (**left**) and temperature (**right**) in Cases 1 and 2 at a running time of t = 1000 s.

In the terrestrial ionosphere, the ionosphere can be divided into the E, F1, and F2 layers. Frequently, the F2 layer splits into two layers during the daytime in the F region of the equatorial ionosphere. This splitting of the F2 layer was first reported as early as the 1940s [34,35]. After many studies on the vertical structure of the terrestrial ionosphere, it is well-known that the splitting of the F2 layer could be caused by the ExB drift and gravity waves. However, the F3 layer, induced by vertical ExB drift, often lasts for more than 1 h [24]. The F2 layer stratification induced by gravity waves usually lasts for about 15–60 min [24].

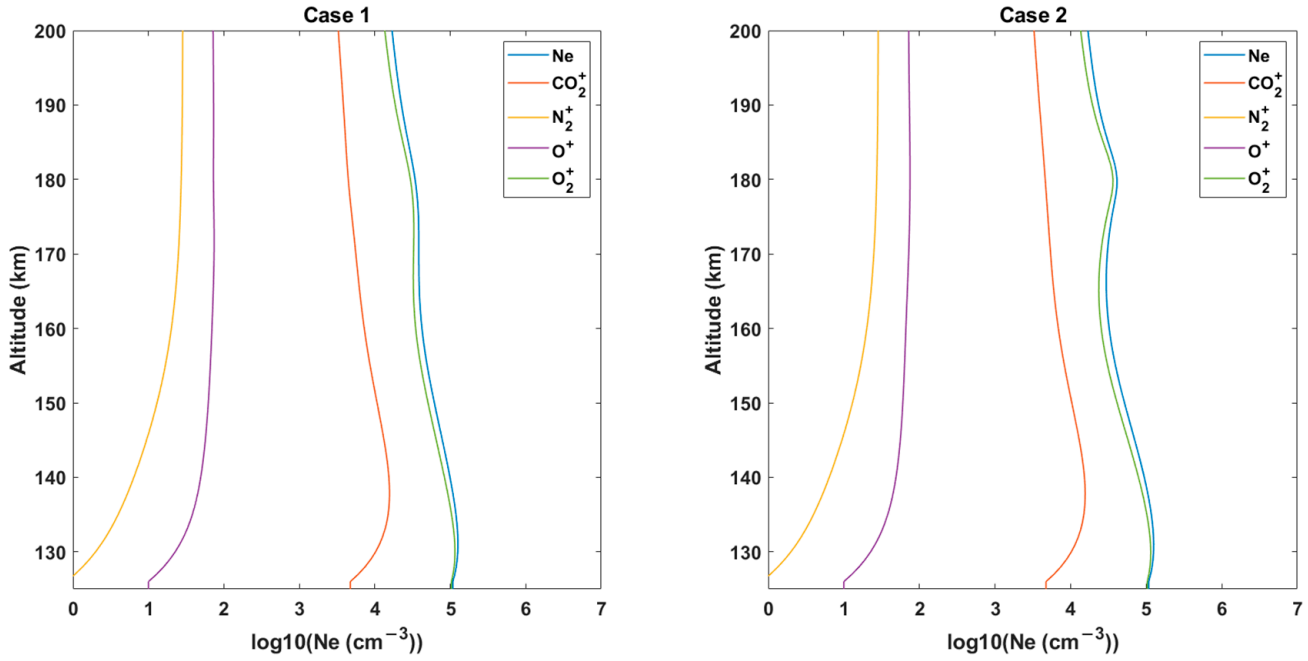

Figure 6. Densities of O_2^+, CO_2^+, O^+, and N_2^+ electrons in Case 1 (**left**) and Case 2 (**right**) at a running time of t = 1000 s.

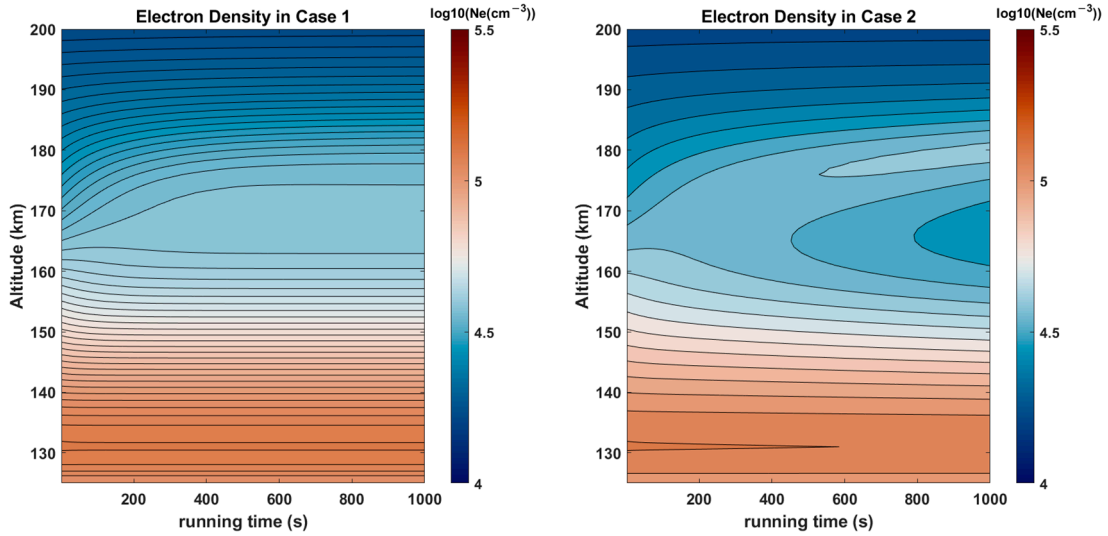

Figure 7. Temporal variations in electron density profiles at running times in Cases 1 and 2.

Subsequently, the new, additional upper layer induced by the ExB drift was called the F3 layer [23]. After many studies about the F3 layer in the terrestrial ionosphere, the physical processes involved in the F3 layer became well-understood. The combined effects of the ExB drift and the meridional neutral wind lift up the F2 layer. The upward drift raises the peak of the ionosphere to a higher altitude with a lower recombination rate, and then the plasma converges in the topside ionosphere to form the F3 layer [23]. At the same time, a new F2 layer could be formed in the original region by the usual photochemical and dynamic effects. The splitting of the F2 layer caused by gravity waves is F2-layer stratification. Although the driving forces of these two phenomena are different, the processes of photoionization and the dynamic processes are similar and comparable. Both can lead to the nonuniform upward drift of plasma in the ionosphere. As a result, a split in the F2 layer could be formed.

The process involved in the transient topside layer in Case 1 is similar to that of F3-layer or F2-layer stratification in the terrestrial ionosphere. It should be noted that, in Figure 4c, the largest upward velocity of plasma is about ~165 km. However, the transient layer is located at about 175 km (see Case 1 in Figure 5). When the upward drift in the Martian ionosphere occurs, the larger upward drift raises the plasma to a higher altitude, and then the plasma starts to converge due to the lesser upward drift or the absence of it. In addition, the recombination loss is also less in the higher altitude. As a result, the transient layer could be formed above the region with the largest upward velocity in the topside Martian ionosphere.

Many studies [8,17,22] have suggested that the enhancement of the electron temperature could play a significant role in the enhancement of the electron density in the topside ionosphere. However, Mukundan et al. [9] found that, in some cases, an enhancement of the electron temperature was not seen when the M3 layer could be observed. In the second case, prior to the disturbed vertical transport of the plasma, we assumed that the electron temperature was in the equilibrium state. Therefore, only the effect of the disturbed vertical transport on the electron temperature was considered in the simulation. It is reasonable to think that the enhancement of the electron temperature could lead to the enhancement of the electron density due to the lower recombination loss. However, the results of this study suggest that the seeding source of the enhancement of the electron density might not be the electron temperature. The transport process of the plasma might be more important in the formation of the transient topside layer. It could lead to plasma convergence due to the nonuniform upward drift. On the other hand, it also could lead to variations in electron temperature. Then, both the plasma convergence and the lesser recombination loss induced by the enhancement of the electron temperature facilitate the formation of the transient topside layer of the Martian ionosphere. Most important, only the nonuniform upward drift could also produce the M3 layer. This can be used to explain why the enhancement of the electron temperature is not seen when the M3 layer can be observed [9].

Could the vertical transport of plasma be present in the topside Martian ionosphere? On Earth, the large-scale electric field in the F region could originate in the E region and the magnetosphere. However, it is well-known that there is no global magnetic field on Mars. Therefore, the electric field in the Martian ionosphere is different from that of the terrestrial ionosphere. To the best of our knowledge, no directly measured electric field in the Martian ionosphere has been reported up until now. Therefore, it seems to be impossible to specify the role of an electric field in the physical mechanism of the M3 layer in the Martian ionosphere. For that reason, the role of an electric field was not considered in this study. However, gravity waves could be observed frequently in the Martian thermosphere [36,37]. As mentioned above, the upward drift of plasma could also be caused by gravity waves in the ionosphere. Yiğit et al. [32] studied the variations of Martian thermospheric gravity-wave activity via MAVEN, and they found that GW activity varies strongly as a function of altitudes, and it reaches a maximum at ~170 km. This region is near the altitude of the transient topside layer. Collinson et al. [38] reported the first extraterrestrial observation of traveling ionospheric disturbances (TIDs) in the Martian ionosphere. TIDs, mostly induced by atmospheric gravity waves, manifest as oscillating waves in the density, velocity, and composition of plasma in the ionosphere. Collinson et al. [38] suggested that gravity waves could drive the vertical motion of ions and produce TIDs in the Martian ionosphere. Jiang et al. [39] also carried out modeling of ionospheric irregularity seeding via variations of neutral winds induced by gravity waves. Tian et al. [40] further studied variations of Martian ionospheric irregularities and suggested that both the upward propagation of atmospheric gravity waves and the downward propagation of the perturbations of solar wind could drive the disturbance of the Martian ionosphere. Therefore, it might be reasonable to think that the vertical drift in the topside Martian ionosphere cannot be ignored when studying the altitudinal structure of the topside ionosphere.

4. Conclusions

In this paper, we present a simulation of the transient topside layer (M3 layer) in the Martian ionosphere. Our results show that the nonuniform upward drift of the plasma might play a crucial role in the formation of the M3 layer in the Martian ionosphere. Vertical drift might be the seeding source of the M3 layer and the enhancement of electron temperature. The vertical transport process could cause not only plasma convergence but also the enhancement of the electron temperature. The lesser recombination loss caused by the enhancement of the electron temperature further facilitates the formation of the M3 layer. Both atmospheric gravity waves from the lower atmosphere and perturbations of topside ionosphere from the upper solar wind could provide seeding sources for the disturbances in the vertical transport of the plasma in the topside Martian ionosphere.

Author Contributions: Data curation, C.J.; methodology, C.J.; model, R.T.; validation, L.W.; investigation, C.J. and R.T.; writing—original draft preparation, C.J.; writing—review and editing, C.J. and R.T.; project administration, C.J.; funding acquisition, C.J. All authors have read and agreed to the published version of the manuscript.

Funding: This research was funded by the National Natural Science Foundation of China (NSFC), grant number 42074184, and 41727804.

Data Availability Statement: The data used in this study are available on Zenodo [41].

Acknowledgments: We are grateful to the editor and reviewers for their assistance in evaluating this paper.

Conflicts of Interest: The authors declare no conflict of interest.

References

1. Patzold, M.; Tellmann, S.; Hansler, B.; Hinson, D.; Schaa, R.; Taylet, G.L. A sporadic third layer in the ionosphere of Mars. *Science* **2005**, *310*, 837–839. [CrossRef] [PubMed]
2. Hinson, D.P.; Simpson, R.A.; Twicken, J.D.; Tyler, G.L.; Flasar, F.M. Initial results from radio occultation measurements with Mars Global Surveyor. *J. Geophys. Res.* **1999**, *104*, 26997–27012. [CrossRef]
3. Jakosky, B.M.; Lin, R.P.; Grebowsky, J.M.; Luhmann, J.G.; Mitchell, D.F.; Beutelschies, G.; Priser, T.; Acuna, M.; Andersson, L.; Baird, D.; et al. The Mars Atmosphere and Volatile Evolution (MAVEN) Mission. *Space Sci. Rev.* **2015**, *195*, 3–48. [CrossRef]
4. Rishbeth, H.; Mendillo, M. Ionospheric layers of Mars and Earth. *Planet. Space Sci.* **2004**, *52*, 849–852. [CrossRef]
5. Grebowsky, J.M.; Benna, M.; Plane, J.M.C.; Collinson, G.A.; Mahaffy, P.R.; Jakosky, B.M. Unique, non-Earthlike, meteoritic ion behavior in upper atmosphere of Mars. *Geophys. Res. Lett.* **2017**, *44*, 3066–3072. [CrossRef]
6. Crismani, M.; Schneider, N.; Plane, J.; Evans, J.S.; Jain, S.K.; Chaffin, M.S.; Carrillo-Sanchez, J.D.; Deighan, J.I.; Yelle, R.V.; Stewart, A.I.F.; et al. Detection of a persistent meteoric metal layer in the Martian atmosphere. *Nature Geosci.* **2017**, *10*, 401–404. [CrossRef]
7. Hanson, W.B.; Sanatani, S.; Zuccaro, D.R. The martian ionosphere as observed by the viking retarding potential analyzers. *J. Geophys. Res.* **1977**, *82*, 4351–4363. [CrossRef]
8. Mayyasi, M.; Withers, P.; Fallows, K. A sporadic topside layer in the ionosphere of Mars from analysis of MGS radio occultation data. *J. Geophys. Res. Space Phys.* **2018**, *123*, 883–900. [CrossRef]
9. Mukundan, V.; Thampi, S.V.; Bhardwaj, A. M3 electron density layer in the dayside ionosphere of Mars: Analysis of MAVEN ROSE observations. *Icarus* **2022**, *384*, 115062. [CrossRef]
10. Zhang, M.H.G.; Luhmann, J.G.; Kliore, A.J.; Kim, J. A post-Pioneer Venus reassessment of the Martian dayside ionosphere as observed by radio occultation methods. *J. Geophys. Res.* **1990**, *95*, 14829–14839. [CrossRef]
11. Lillis, R.J.; Fillingim, M.O.; Peticolas, L.M.; Brain, D.A.; Lin, R.P.; Bougher, S.W. Nightside ionosphere of mars: Modeling the effects of crustal magnetic fields and electron pitch angle distributions on electron impact ionization. *J. Geophys. Res.* **2009**, *114*, E11009. [CrossRef]
12. Terada, N.; Machida, S.; Shinagawa, H. Global hybrid simulation of the Kelvin-Helmholtz instability at the Venus ionopause. *J. Geophys. Res.* **2002**, *107*, 1471. [CrossRef]
13. Zhang, Z.; Orosei, R.; Huang, Q.; Zhang, J. Topside of the Martian ionosphere near the terminator: Variation with season and solar zenith angle and implications for the origin of the transient layers. *Icarus* **2015**, *251*, 12–25. [CrossRef]
14. Kopf, A.J.; Gurnett, D.A.; DiBraccio, G.A.; Morgan, D.D.; Halekas, J.S. The transient topside layer and associated current sheet in the ionosphere of Mars. *J. Geophys. Res. Space Phys.* **2017**, *122*, 5579–5590. [CrossRef]
15. Shinagawa, H.; Cravens, T. The ionospheric effects of a weak intrinsic magnetic field at Mars. *J. Geophys. Res.* **1992**, *97*, 1027–1035. [CrossRef]

16. Collinson, G.A.; McFadden, J.; Grebowsky, J.; Mitchell, D.; Lillis, R.; Withers, P.; Vogt, M.F.; Benna, M.; Espley, J.; Jakosky, B. Constantly forming sporadic E-like layers and rifts in the martian ionosphere and their implications for earth. *Nat. Astron.* **2020**, *4*, 486–491. [CrossRef]
17. Fox, J.L.; Yeager, K.E. Morphology of the near-terminator Martian ionosphere: A comparison of models and data. *J. Geophys. Res.* **2006**, *111*, A10309. [CrossRef]
18. Andrews, D.J.; André, M.; Opgenoorth, H.J.; Edberg, N.T.; Diéval, C.; Duru, F.; Gurnett, D.A.; Morgan, D.; Witasse, O. Oblique reflections in the Mars Express MARSIS data set: Stable density structures in the Martian ionosphere. *J. Geophys. Res. Space Phys.* **2014**, *119*, 3944–3960. [CrossRef]
19. Wang, J.-S.; Nielsen, E. Possible hydrodynamic waves in the topside ionospheres of Mars and Venus. *J. Geophys. Res.* **2002**, *107*, SIA-2. [CrossRef]
20. Wang, J.-S.; Nielsen, E. Wavelike structures in the Martian topside ionosphere observed by Mars Global Surveyor. *J. Geophys. Res.* **2003**, *108*, 5078. [CrossRef]
21. Wang, X.-D.; Wang, J.-S.; Nielsen, E.; Zou, H. "Hook" structure in MARSIS ionogram and its interpretation. *Geophys. Res. Lett.* **2009**, *36*, L13103. [CrossRef]
22. Mendillo, M.; Phillips, S.R.; Narvaez, C.; Mayyasi, M.; Thiemann, E.; Benna, M.; Eparvier, F.; Chamberlin, P.; Mahaffy, P.; Andersson, L. On the altitude patterns of photo-chemical-equilibrium in the Martian ionosphere: A special role for electron temperature. *J. Geophys. Res. Space Phys.* **2021**, *126*, e2020JA028366. [CrossRef]
23. Balan, N.; Bailey, G.J.; Abdu, M.A.; Oyama, K.I.; Richards, P.G.; MacDougall, J.; Batista, I.S. Equatorial plasma fountain and its effects over three locations: Evidence for an additional layer, the F_3 layer. *J. Geophys. Res.* **1997**, *102*, 2047–2056. [CrossRef]
24. Jiang, C.; Yang, G.; Liu, J.; Zhao, Z. Reply to Comment by Lynn et al. on "A study of the F2 layer stratification on ionograms using a simple model of TIDs". *J. Geophys. Res. Space Phys.* **2020**, *125*, e2020JA027785. [CrossRef]
25. Jiang, C.; Yang, G.; Liu, J.; Zhao, Z. A study of the F2 layer stratification on ionograms using a simple model of TIDs. *J. Geophys. Res. Space Phys.* **2019**, *124*, 1317–1327. [CrossRef]
26. Schunk, R.; Nagy, A. *Ionospheres: Physics, Plasma Physics, and Chemistry*; Cambridge University Press: New York, NY, USA, 2000.
27. Tobiska, W.K. SOLAR2000 Irradiances for Climate Change Research, Aeronomy and Space System Engineering. *Adv. Space Res.* **2004**, *34*, 1736–1746. [CrossRef]
28. Verner, D.A.; Yakovlev, D.G. Analytic FITS for Partial Photoionization Cross Sections. *Astron. Astrophys. Suppl. Ser.* **1995**, *109*, 125–133.
29. Verner, D.A.; Ferland, G.J.; Korista, K.T.; Yakovlev, D.G. Atomic Data for Astrophysics. II. New Analytic Fits for Photoionization Cross Sections of Atoms and Ions. *arXiv* **1996**. [CrossRef]
30. Morgan, D.D.; Gurnett, D.A.; Kirchner, D.L.; Fox, J.L.; Nielsen, E.; Plaut, J.J. Variation of the Martian ionospheric electron density from Mars Express radar soundings. *J. Geophys. Res.* **2008**, *113*, A09303. [CrossRef]
31. Vogt, M.F.; Withers, P.; Fallows, K.; Andersson, L.; Girazian, Z.; Mahaffy, P.R.; Benna, M.; Elrod, M.K.; Connerney, J.E.; Espley, J.R.; et al. MAVEN observations of dayside peak electron densities in the ionosphere of Mars. *J. Geophys. Res. Space Phys.* **2017**, *122*, 891–906. [CrossRef]
32. Yiğit, E.; Medvedev, A.S.; Hartogh, P. Variations of the Martian Thermospheric Gravity-wave Activity during the Recent Solar Minimum as Observed by MAVEN. *Astrophys. J.* **2021**, *920*, 69. [CrossRef]
33. Matta, M.; Galand, M.; Moore, L.; Mendillo, M.; Withers, P. Numerical simulations of ion and electron temperatures in the ionosphere of Mars: Multiple ions and diurnal variations. *Icarus* **2014**, *227*, 78–88. [CrossRef]
34. Bailey, D.K. The geomagnetic nature of the F2 layer longitude effect. *J. Geophys. Res.* **1948**, *53*, 35–39. [CrossRef]
35. Sen, H.Y. Stratification of the F2 layer of the ionosphere over Singapore. *J. Geophys. Res.* **1949**, *54*, 363–366. [CrossRef]
36. Yiğit, E.; England, S.L.; Liu, G.; Medvedev, A.S.; Mahaffy, P.R.; Kuroda, T.; Jakosky, B.M. High-altitude gravity waves in the Martian thermosphere observed by MAVEN/NGIMS and modeled by a gravity wave scheme. *Geophys. Res. Lett.* **2015**, *42*, 8993–9000. [CrossRef]
37. Terada, N.; Leblanc, F.; Nakagawa, H.; Medvedev, A.S.; Yiğit, E.; Kuroda, T.; Hara, T.; England, S.L.; Fujiwara, H.; Terada, K.; et al. Global distribution and parameter dependences of gravity wave activity in the Martian upper thermosphere derived from MAVEN/NGIMS observations. *J. Geophys. Res. Space Phys.* **2017**, *122*, 2374–2397. [CrossRef]
38. Collinson, G.; McFadden, J.; Mitchell, D.; Grebowsky, J.; Benna, M.; Espley, J.; Jakosky, B. Traveling ionospheric disturbances at Mars. *Geophys. Res. Lett.* **2019**, *46*, 4554–4563. [CrossRef]
39. Jiang, C.; Yokoyama, T.; Wei, L.; Yang, G.; Zhao, Z. Nonlinear Simulation of Ionospheric Irregularities at Mars. *Astrophys. J.* **2021**, *909*, 47. [CrossRef]
40. Tian, R.; Jiang, C.; Yang, G.; Yin, W.; Zhang, Y.; Zhao, Z. Solar Cycle and Seasonal Variability of Martian Ionospheric Irregularities from Mars Atmosphere and Volatile Evolution Observations. *Astrophys. J.* **2022**, *931*, 18. [CrossRef]
41. Jiang, C. *Chuajiang/Simulation-of-Transient-Topside-Layer-in-the-Martian-Ionosphere: V1*; Version v1; Zenodo: Geneva, Switzerland, 2022. [CrossRef]